Supplemental Material for:
From pore collapse to crystal growth: ultrafast laser-induced stishovite formation in nanoporous silica

Aram Yedigaryan[1], Mohamed Yaseen Noor[2], Elena Kachan[1], Gabriel Calderon[2], Jinwoo Hwang[2], Enam Chowdhury[2], Jean-Philippe Colombier[1]

[1] *Université Jean Monnet, CNRS, Institut d'Optique Graduate School, Laboratoire Hubert Curien UMR 5516, Saint-Etienne F-42023, France and*

[2] *Department of Materials Science and Engineering, The Ohio State University, 140W 19th Avenue, Columbus, 43210, Ohio, United States*

(Dated: July 28, 2026)

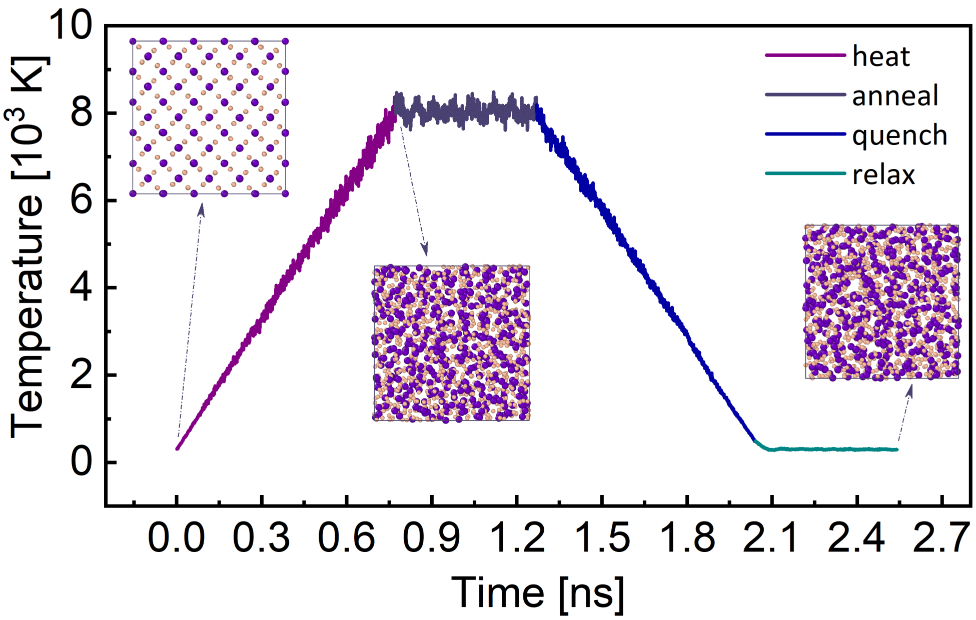

FIG. S1. Temporal evolution of temperature during the amorphization of stishovite. A standard heat-anneal-quench-relax protocol is used with canonical ensemble. The annealing stage is applied after heating to ensure a total removal of crystalline memory from the already amorphized system. A relaxation stage is applied to remove any residual stress after the quench. The snapshots show the initial ordered (c-axis) and the disordered configurations during the amorphization process.

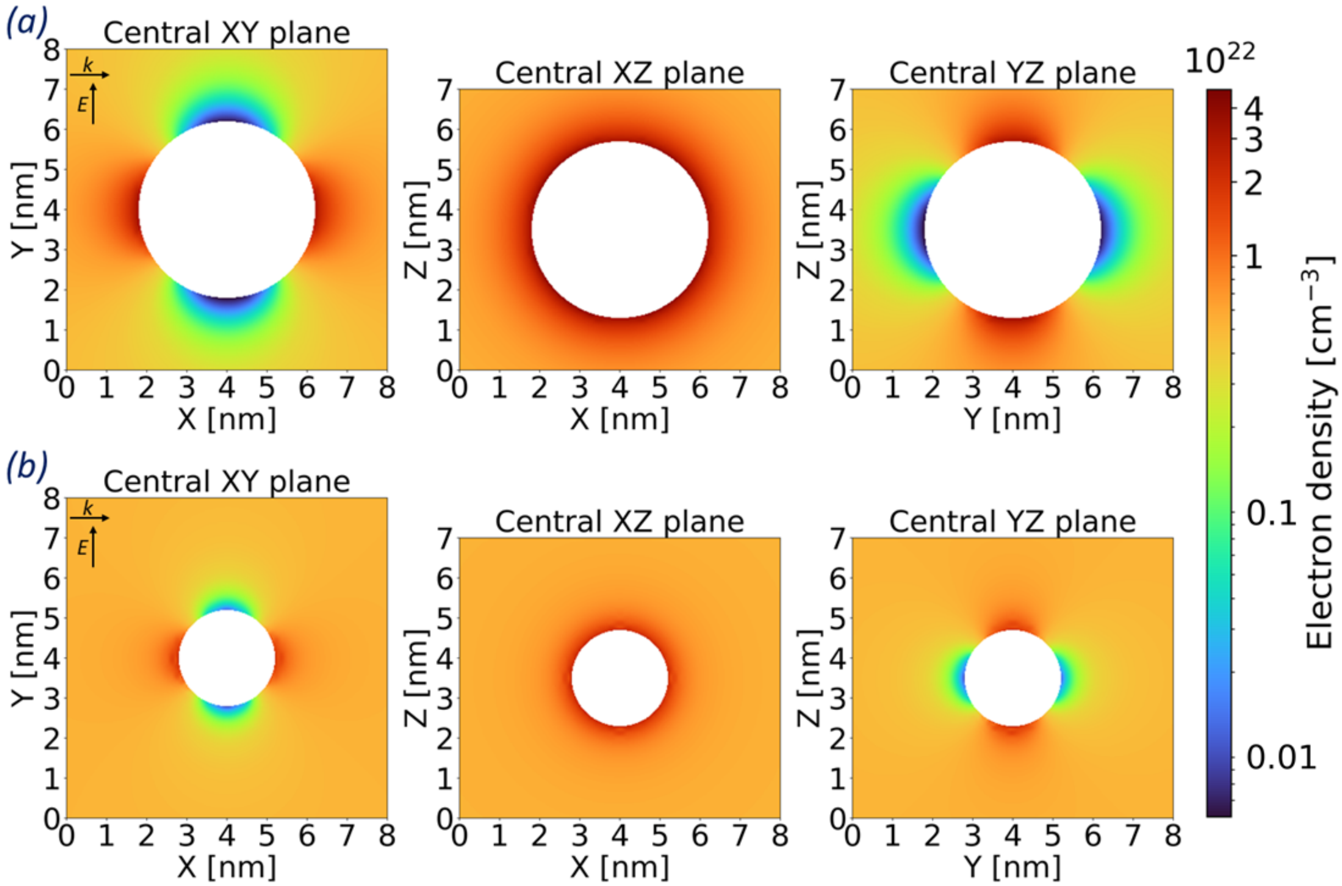

FIG. S2. Central slices of free-electron density distribution after laser irradiation, smoothened for better visualization, for the structure with a (a) 4-nm-pore and (b) 2-nm-pore. The free-electron density is strongly modulated by the presence of the pore for both pore sizes, reaching a maximum value right at the pore surface boundary of approximately 4×10^{22} cm^{-3}. The highest electron densities are localized at the pore surface regions aligned with the laser polarization direction. The discontinuity in permittivity at the dielectric-pore interface leads to local electric field amplification, which enhances nonlinear ionization processes and results in higher electron densities near the pore boundary.

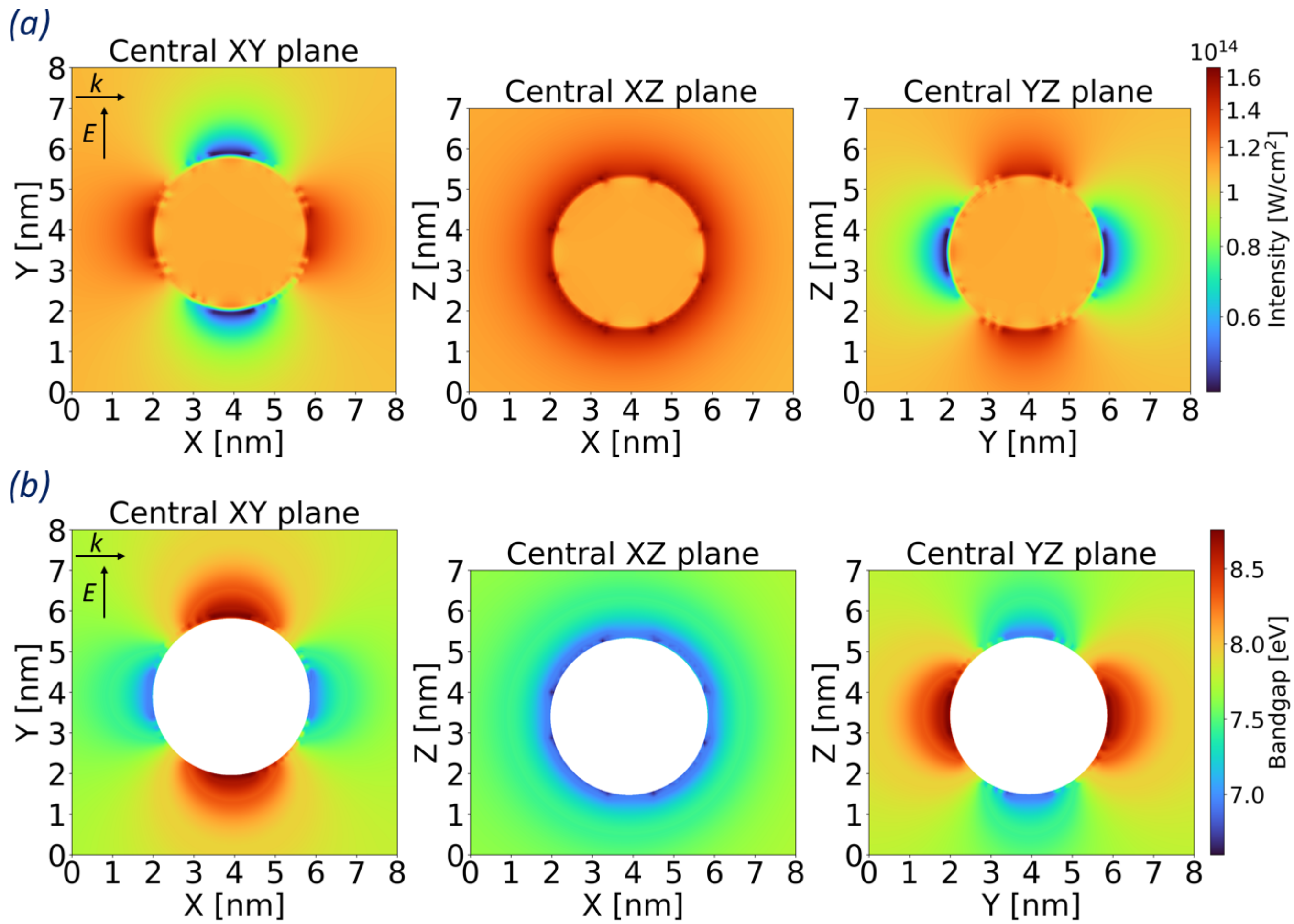

FIG. S3. (a) Smoothened intensity spatial distribution of 4-nm-pore structure taken from FDTD data when the laser pulse intensity was at its peak. (b) The corresponding bandgap distribution obtained by mapping the local intensity to the intensity-dependent bandgap (top panel in Fig. 2 of main text). The maximum local intensity exceeds the incident peak value by a factor of around 1.65 in the hottest spots of the pore boundaries, indicating significant near-field enhancement at silica interface. In the background, the bandgap decreases from the ground-state 8.9 eV to around 7.9 eV, while at the hottest spots along the pore boundary it further decreases to approximately 6.6 eV. This localized bandgap shrinkage is confined to a narrow region around the interface, corresponding to the steep spatial gradients of the electromagnetic field. Even at intensities close to approximately 4.5×10^{13} W/cm^2 $- 1.65 \times 10^{14}$ W/cm^2 range, relevant to our simulations, the dynamic bandgap increases the calculated rate at the hottest spots of the pore boundaries by a factor of up to about 6 compared to the static-bandgap case, indicating that field-driven gap renormalization significantly amplifies free-carrier generation. One should also note that while the ratio of ionization rate between the pore boundary and background homogeneous region was approximately 4 in case of static bandgap, the same ratio increased to approximately 10 in case of dynamic bandgap.

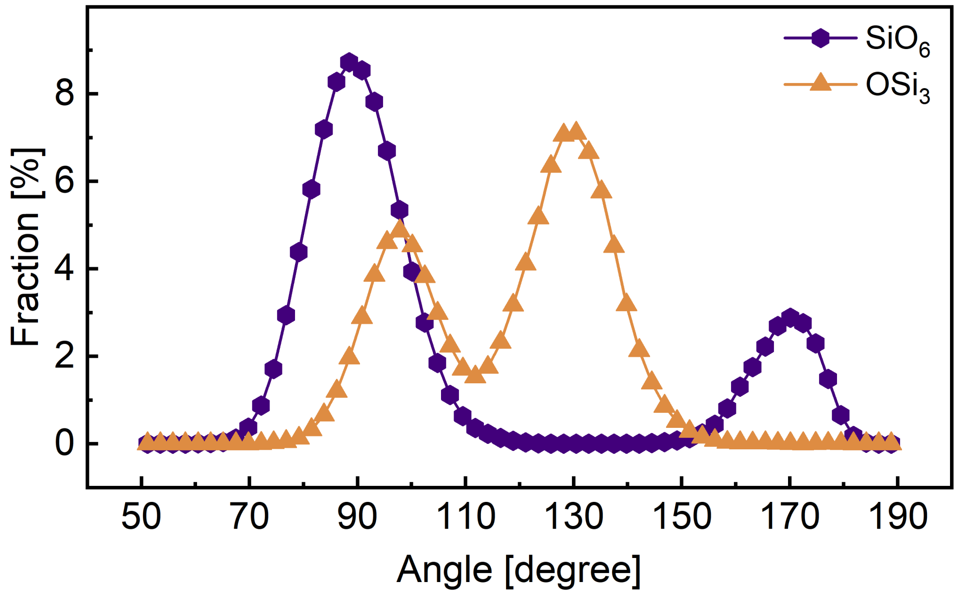

FIG. S4. Bond-angle distribution for O-Si-O and Si-O-Si angles within SiO_6 and OSi_3 coordination units of the crystallized system 2 ns after irradiation. The peaks at 90° and 170° of SiO_6 unit correspond to adjacent and trans ligands, respectively. Similarly, the peaks at 97° and 130° of OSi_3 unit show the edge sharing and corner-sharing connections.

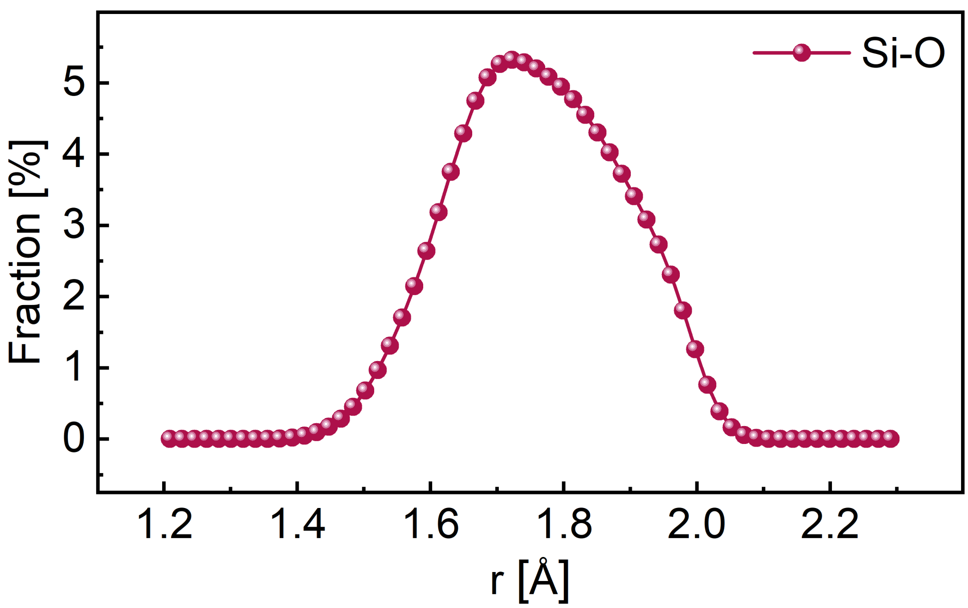

FIG. S5. Si-O bond-length distribution, peaked around 1.73 Å, within SiO_6 coordination units in the crystallized system at a final pressure of 27 GPa.

Supplemental Videos

Video S1 —— Nanopore collapse within a picosecond following laser pulse irradiation.
Video S2 —— Crystallization of silica to stishovite within a nanosecond following laser pulse irradiation.